NASA/TM-2003-212029

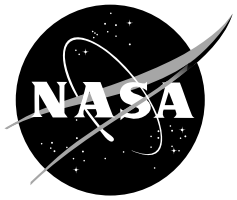

# Flight Investigation of Prescribed Simultaneous Independent Surface Excitations for Real-Time Parameter Identification

*Timothy R. Moes and Mark S. Smith*
*NASA Dryden Flight Research Center*
*Edwards, California*

*Eugene A. Morelli*
*NASA Langley Research Center*
*Hampton, Virginia*

**October 2003**

## The NASA STI Program Office…in Profile

Since its founding, NASA has been dedicated to the advancement of aeronautics and space science. The NASA Scientific and Technical Information (STI) Program Office plays a key part in helping NASA maintain this important role.

The NASA STI Program Office is operated by Langley Research Center, the lead center for NASA's scientific and technical information. The NASA STI Program Office provides access to the NASA STI Database, the largest collection of aeronautical and space science STI in the world. The Program Office is also NASA's institutional mechanism for disseminating the results of its research and development activities. These results are published by NASA in the NASA STI Report Series, which includes the following report types:

- TECHNICAL PUBLICATION. Reports of completed research or a major significant phase of research that present the results of NASA programs and include extensive data or theoretical analysis. Includes compilations of significant scientific and technical data and information deemed to be of continuing reference value. NASA's counterpart of peer-reviewed formal professional papers but has less stringent limitations on manuscript length and extent of graphic presentations.

- TECHNICAL MEMORANDUM. Scientific and technical findings that are preliminary or of specialized interest, e.g., quick release reports, working papers, and bibliographies that contain minimal annotation. Does not contain extensive analysis.

- CONTRACTOR REPORT. Scientific and technical findings by NASA-sponsored contractors and grantees.

- CONFERENCE PUBLICATION. Collected papers from scientific and technical conferences, symposia, seminars, or other meetings sponsored or cosponsored by NASA.

- SPECIAL PUBLICATION. Scientific, technical, or historical information from NASA programs, projects, and mission, often concerned with subjects having substantial public interest.

- TECHNICAL TRANSLATION. English-language translations of foreign scientific and technical material pertinent to NASA's mission.

Specialized services that complement the STI Program Office's diverse offerings include creating custom thesauri, building customized databases, organizing and publishing research results…even providing videos.

For more information about the NASA STI Program Office, see the following:

- Access the NASA STI Program Home Page at ***http://www.sti.nasa.gov***

- E-mail your question via the Internet to help@sti.nasa.gov

- Fax your question to the NASA Access Help Desk at (301) 621-0134

- Telephone the NASA Access Help Desk at (301) 621-0390

- Write to:
  NASA Access Help Desk
  NASA Center for AeroSpace Information
  7121 Standard Drive
  Hanover, MD 21076-1320

NASA/TM-2003-212029

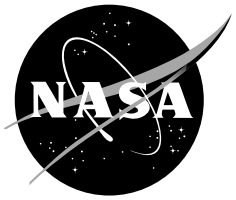

# Flight Investigation of Prescribed Simultaneous Independent Surface Excitations for Real-Time Parameter Identification

*Timothy R. Moes and Mark S. Smith*
*NASA Dryden Flight Research Center*
*Edwards, California*

*Eugene A. Morelli*
*NASA Langley Research Center*
*Hampton, Virginia*

National Aeronautics and
Space Administration

Dryden Flight Research Center
Edwards, California 93523-0273

**October 2003**

## NOTICE

Use of trade names or names of manufacturers in this document does not constitute an official endorsement of such products or manufacturers, either expressed or implied, by the National Aeronautics and Space Administration.

Available from the following:

NASA Center for AeroSpace Information (CASI)
7121 Standard Drive
Hanover, MD 21076-1320
(301) 621-0390

National Technical Information Service (NTIS)
5285 Port Royal Road
Springfield, VA 22161-2171
(703) 487-4650

## ABSTRACT

Near real-time stability and control derivative extraction is required to support flight demonstration of Intelligent Flight Control System (IFCS) concepts being developed by NASA, academia, and industry. Traditionally, flight maneuvers would be designed and flown to obtain stability and control derivative estimates using a postflight analysis technique. The goal of the IFCS concept is to be able to modify the control laws in real time for an aircraft that has been damaged in flight. In some IFCS implementations, real-time parameter identification (PID) of the stability and control derivatives of the damaged aircraft is necessary for successfully reconfiguring the control system. This report investigates the usefulness of Prescribed Simultaneous Independent Surface Excitations (PreSISE) to provide data for rapidly obtaining estimates of the stability and control derivatives. Flight test data were analyzed using both equation-error and output-error PID techniques. The equation-error PID technique is known as Fourier Transform Regression (FTR) and is a frequency-domain real-time implementation. Selected results were compared with a time-domain output-error technique. The real-time equation-error technique combined with the PreSISE maneuvers provided excellent derivative estimation in the longitudinal axis. However, the PreSISE maneuvers as presently defined were not adequate for accurate estimation of the lateral-directional derivatives.


## NOMENCLATURE

### Acronyms

| | |
|---|---|
| CG | center of gravity |
| DCS | Dynamic Cell Structure |
| FTR | Fourier Transform Regression |
| IFCS | Intelligent Flight Control System |
| PID | parameter identification |
| PreSISE | Prescribed Simultaneous Independent Surface Excitations |

### Symbols

| | |
|---|---|
| $a_n$ | normal acceleration (positive up), $g$ |
| $a_y$ | lateral acceleration (positive toward the right), $g$ |
| $A$ | amplitude parameter of PreSISE definition, deg |
| $b$ | wing span, 42.7 ft |
| $c$ | reference chord, 15.94 ft |
| $C_l$ | rolling-moment coefficient |
| $C_m$ | pitching-moment coefficient |
| $C_n$ | yawing-moment coefficient |
| $C_N$ | normal-force coefficient |

| | |
|---|---|
| $C_Y$ | side-force coefficient |
| $g$ | acceleration of gravity, 32.174 ft/sec$^2$ |
| $I_x$ | roll moment of inertia, slug-ft$^2$ |
| $I_{xz}$ | cross product of inertia, slug-ft$^2$ |
| $I_y$ | pitch moment of inertia, slug-ft$^2$ |
| $I_z$ | yaw moment of inertia, slug-ft$^2$ |
| $m$ | aircraft mass, slug |
| M | Mach number |
| $p$ | roll rate, deg/sec |
| $q$ | pitch rate, deg/sec |
| $\bar{q}$ | dynamic pressure, psf |
| $r$ | yaw rate, deg/sec |
| $R$ | conversion factor, 57.2958 deg/rad |
| $S$ | wing area, 608 ft$^2$ |
| $t$ | time, sec |
| $V$ | true airspeed, ft/sec |
| $\boldsymbol{X}$ | vector of regressors with trim value removed |
| $Y$ | force or moment coefficient with trim value removed |
| $\alpha$ | angle of attack, deg |
| $\beta$ | angle of sideslip, deg |
| $\delta_a$ | aileron deflection, deg |
| $\delta_c$ | symmetric canard deflection, deg |
| $\delta_{dc}$ | differential canard deflection, deg |
| $\delta_{dh}$ | differential stabilator deflection, deg |
| $\delta_e$ | elevator (symmetric stabilator) deflection, deg |
| $\delta_r$ | rudder deflection, deg |
| $\phi$ | roll angle, deg |
| $\theta$ | pitch angle, deg |
| $\xi$ | stability and control derivative parameter vector |
| $\cdot$ | time rate of change of a parameter |

# INTRODUCTION

NASA, industry, and academia are currently developing Intelligent Flight Control System (IFCS) concepts. The goal of IFCS is the ability to modify in real time the flight control system of an aircraft that has been damaged in flight (such as battle damage, weather, or system failure). NASA Dryden Flight Research Center (Edwards, California) has begun flight tests to demonstrate an IFCS approach that includes near real-time estimation of aerodynamic stability and control derivatives. Although not yet implemented on the aircraft, figure 1 shows that in this concept, stability and control derivative estimates are supplied to an adaptive online-learning neural network known as Dynamic Cell Structure (DCS).[1] The DCS continuously chooses a set of stability and control derivatives for the current flight condition and passes that information to a reconfigurable flight control system.

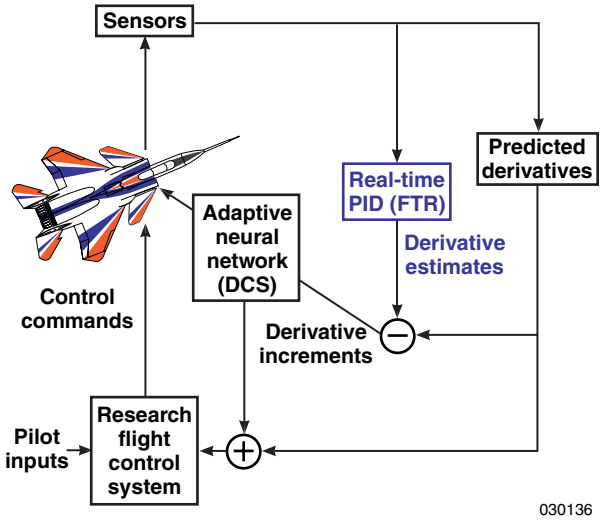


Figure 1. Schematic of the real-time PID role for IFCS research.

The stability and control derivative estimation process is known as parameter identification (PID) or parameter estimation. This process involves identifying the aerodynamic stability and control characteristics from measured aircraft responses and control-surface movements. Traditionally, control surfaces were moved individually by pilot stick and rudder inputs.[2] With modern highly augmented aircraft, a simple stick or rudder input could result in multiple control-surface actuations that are highly correlated in time and shape. These correlated actuations make the individual control effectiveness values unidentifiable from PID analysis. To solve this problem, previous flight projects have used programmed control-surface inputs run by the aircraft flight control computer in which each control surface was independently actuated in sequence so that all control-surface effectiveness values could be identified.

For an aircraft with multiple control surfaces, this input could take tens of seconds to complete.[3] For the IFCS requirement of rapid derivative identification after some unknown system damage, a new programmed test input was desired that would move all surfaces simultaneously but still independently from each other. Moving the control surfaces simultaneously, but in different ways, makes it possible to collect data for all the control-surface effectiveness values at the same time, instead of having to sequence the inputs, which takes longer. The Prescribed Simultaneous Independent Surface Excitations (PreSISE) were developed to meet this requirement.[4] Sinusoidal inputs were sent to each set of control effectors at different frequencies so that aircraft responses could be correlated to specific control surfaces.[5]

In this report, both output-error and equation-error PID techniques were used to analyze the flight data from the PreSISE inputs. Output-error methods[6] are typically used in postflight analysis by iteratively varying the derivative estimates until time histories from integrated equations of motion fit the measured response time histories. Equation-error techniques do not involve integrating equations of motion but can be thought of as least-square fits to measured data in the equations of motion. Equation error was chosen for real-time implementation since it is not an iterative process resulting from linear dependency of the output on the parameters in the equation being fit. In the equation-error technique detailed in this report, measured aircraft response parameters were used to compute force and moment coefficients. Force and moment derivative estimates were then obtained that minimized the squared error between measured and estimated force and moment coefficients. In particular, a real-time frequency-domain equation-error PID technique[7,8] was developed to support the future IFCS goal of online real-time parameter identification. This equation-error technique is known as Fourier Transform Regression (FTR). An output-error PID technique in the time domain, known as pEst,[9] was used to compare with FTR.

This report presents results from the flight tests. It details the pros and cons of the PID algorithms and shows the effectiveness of the PreSISE inputs for rapid stability and control derivative identification. Measured flight data from pilot-input maneuvering was used to assess the accuracy of both FTR and pEst estimated derivatives obtained from the PreSISE maneuvers.

## AIRCRAFT DESCRIPTION

A pre-production Boeing (St. Louis, Missouri) F-15B airplane that has been highly modified to support various test programs was used for this research. The most visible modification is the inclusion of a set of canards near the pilot station (fig. 2). The canards are a set of modified horizontal stabilators from Boeing's F-18 aircraft. The purpose of the canard addition was to increase maneuverability and load capability. An additional effect of the canards was to cause the airplane to be statically unstable in the longitudinal axis at most subsonic speeds. The propulsion system consists of two Pratt & Whitney (West Palm Beach, Florida) F100-PW-229 engines, each equipped with an axisymmetric thrust vectoring pitch/yaw balance beam nozzle. The thrust vectoring feature, however, was not used during the flight test detailed in this report.

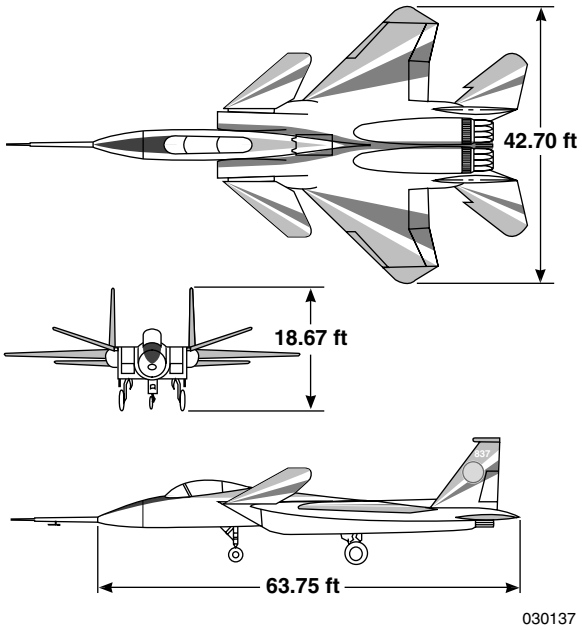


Figure 2. Three-view drawing of F-15 IFCS aircraft with major dimensions shown.

## Control Surfaces

The airplane has five pairs of control surfaces: canards, ailerons, trailing-edge flaps, stabilators, and rudders. Flaps and aileron droop are manually set by the pilot and only used for takeoff and landing configurations. Conventional pitch control is provided by symmetric deflection of the all-moving horizontal stabilators and canards. Roll control uses aileron and differential stabilator. Directional control is provided by rudder and differential canard deflection. The following control-surface deflections definitions have *trailing-edge down* defined as positive deflections for wing, canard, and stabilator surfaces; and *trailing-edge left* defined as positive for the rudder surfaces:

Pitch effectors:

$$\delta_c = 0.5(\delta_{c_{Left}} + \delta_{c_{Right}})$$

$$\delta_e = 0.5(\delta_{e_{Left}} + \delta_{e_{Right}})$$

Yaw/Roll effectors:

$$\delta_{dc} = \delta_{c_{Left}} - \delta_{c_{Right}}$$

$$\delta_a = \delta_{a_{Left}} - \delta_{a_{Right}}$$

$$\delta_{dh} = \delta_{e_{Left}} - \delta_{e_{Right}}$$

$$\delta_r = 0.5(\delta_{r_{Left}} + \delta_{r_{Right}})$$

For the nominal flight control system, pilot stick and rudder inputs result in high correlation between the symmetric canard and angle of attack ($\alpha$), rudder and differential canard, and differential stabilator and aileron. Figure 3 shows this high correlation in a typical time history from pilot-input doublets. Analysis showed that the symmetric canard and angle of attack were nominally correlated 93 percent, rudder and differential canard were correlated 99 percent, and the differential stabilator and aileron were correlated 100 percent. Given these high levels of correlated inputs, it would be impossible with pilot-input maneuvers to distinguish, for example, between rolling moment generated by the aileron and rolling moment generated by the differential stabilator. Consequently, the complete stability and control derivative set cannot be obtained with pilot-input maneuvers.

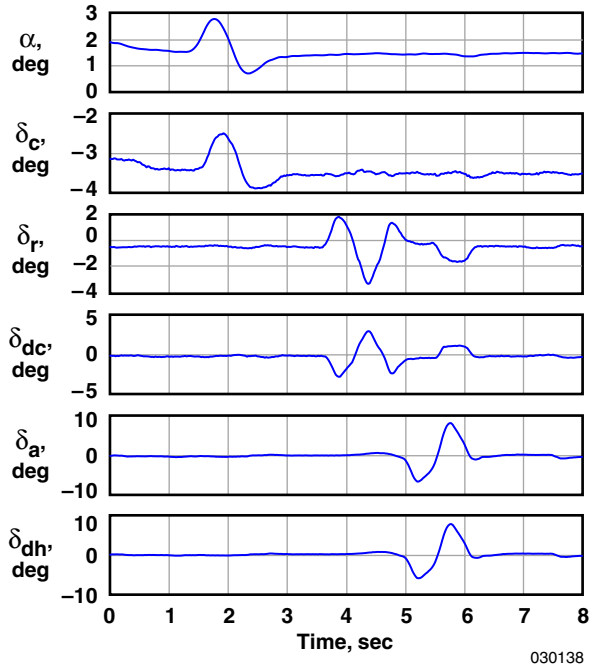


Figure 3. Doublet time history showing correlated data (Mach 1.2 at 32,000 ft).

## Instrumentation and Data Acquisition

The F-15 airplane was equipped with a complete set of airdata, inertial, control-surface position, and mass property instrumentation. A research noseboom was installed and calibrated for free-stream pitot-static and flow angle measurements. A research quality inertial instrumentation package consisting of three-axis linear accelerometer and angular rate measurements was installed. Inertial pitch and bank angle measurements were obtained from the aircraft inertial navigation system from the Military Standard 1553 multiplex databus. The data analysis accounted for time latencies associated with the 1553 data. Analog control-surface position measurements were obtained from actuator measurements. Fuel quantity measurements were obtained from the three fuselage and two wing tanks. Fuel measurements were used to compute total airplane weight, center of gravity (CG), and mass moments of inertia. The CG location was used to account for the fact that the linear accelerometer and flow angle instrumentation were not located at the CG and the measurements were affected by airplane angular rates.

Mass properties were averaged over the duration of each maneuver and were assumed constant for PID analysis. Angular accelerations were not measured. The PID algorithms computed angular acceleration from angular rate measurements.

## Aircraft Simulation

A full six-degree-of-freedom nonlinear batch simulation was used to develop and test the PID algorithms and control-surface inputs used in this study. A linearizer incorporated into the simulation was used to obtain predicted stability and control derivatives at the flight test conditions. These predictions were used as initial guesses for the output-error technique. The simulator was also used to obtain CG and mass moments of inertia based on flight-measured fuel distributions and preflight weight and balance.

# AERODYNAMIC MODEL

The aerodynamic model to be identified from flight tests consisted of a linear model for the nondimensional force and moment coefficients in terms of partial derivatives with respect to state and control variables. The linear expansions of the longitudinal aerodynamic coefficients are:

$$C_N = C_{N_b} + C_{N_\alpha}\alpha + \frac{c}{2VR}C_{N_q}q + C_{N_{\delta_c}}\delta_c + C_{N_{\delta_e}}\delta_e \tag{1}$$

$$C_m = C_{m_b} + C_{m_\alpha}\alpha + \frac{c}{2VR}C_{m_q}q + C_{m_{\delta_c}}\delta_c + C_{m_{\delta_e}}\delta_e \tag{2}$$

The moment reference for the nonlinear simulation is at 25.65 percent *c*, which is at fuselage station 557.2. The coefficient with the subscript "*b*" is a linear extrapolation of the angle-of-attack derivative from the average angle of attack of the maneuver to 0° angle of attack.[6] Axial-force coefficients were not used in this analysis since the axial-force derivatives do not significantly affect flying qualities and since it is generally difficult to get good estimates of axial-force derivatives without thrust measurements.

The linear expansions of the lateral-directional aerodynamic coefficients are:

$$C_Y = C_{Y_b} + C_{Y_\beta}\beta + \frac{b}{2VR}(C_{Y_p}p + C_{Y_r}r) + C_{Y_{\delta_r}}\delta_r + C_{Y_{\delta_{dc}}}\delta_{dc} + C_{Y_{\delta_a}}\delta_a + C_{Y_{\delta_{dh}}}\delta_{dh} \tag{3}$$

$$C_l = C_{l_b} + C_{l_\beta}\beta + \frac{b}{2VR}(C_{l_p}p + C_{l_r}r) + C_{l_{\delta_r}}\delta_r + C_{l_{\delta_{dc}}}\delta_{dc} + C_{l_{\delta_a}}\delta_a + C_{l_{\delta_{dh}}}\delta_{dh} \tag{4}$$

$$C_n = C_{n_b} + C_{n_\beta}\beta + \frac{b}{2VR}(C_{n_p}p + C_{n_r}r) \tag{5}$$
$$+ C_{n_{\delta_r}}\delta_r + C_{n_{\delta_{dc}}}\delta_{dc} + C_{n_{\delta_a}}\delta_a + C_{n_{\delta_{dh}}}\delta_{dh}$$

The coefficient with the subscript "*b*" is a linear extrapolation of the angle-of-sideslip derivative from the average angle of sideslip ($\beta$) of the maneuver to 0° angle of sideslip. Since the expressions in equations (1)–(5) are really Taylor series expansions, the regressor quantities multiplying each stability and control derivative are actually perturbations from the trim condition.

## METHODS OF ANALYSIS

This section defines the equation-error and output-error techniques used to obtain the stability and control derivative estimates.

### Equation Error

Equation-error analysis assumes the measurements of aircraft states and control-surface positions are perfect and that any errors are in the equation (or model) that defines the dynamics. Aircraft nondimensional force and moment coefficients are calculated using measured inertial quantities and the following nonlinear equations:

$$C_N = a_n mg / \bar{q}S \tag{6}$$

$$C_m = [\dot{q}I_y R - (r^2 - p^2)I_{xz} - rp(I_z - I_x)] / \bar{q}ScR^2 \tag{7}$$

$$C_Y = a_y mg / \bar{q}S \tag{8}$$

$$C_l = [\dot{p}I_x R - \dot{r}I_{xz}R - qr(I_y - I_z) - pqI_{xz}] / \bar{q}SbR^2 \tag{9}$$

$$C_n = [-\dot{p}I_{xz}R + \dot{r}I_z R - pq(I_x - I_y) + qrI_{xz}] / \bar{q}SbR^2 \tag{10}$$

Angular accelerations were not measured in flight but were estimated from angular rate measurements. Since PID involves identifying derivatives and not total forces and moments, trim conditions are subtracted from equations (1)–(5); and with some rearranging, a linear system can be formed for each force and moment coefficient in the form of:

$$Y(t) = \boldsymbol{X}(t)\xi \tag{11}$$

where, using the normal force coefficient as an example:

$$Y(t) = C_N(t) - C_{N_{trim}}$$

$$\xi = \begin{bmatrix} C_{N_\alpha} \\ C_{N_q} \\ C_{N_{\delta_c}} \\ C_{N_{\delta_e}} \end{bmatrix} \qquad \boldsymbol{X}(t) = \begin{bmatrix} \alpha(t) - \alpha_{trim} \\ \frac{c}{2RV} q(t) \\ \delta_c(t) - \delta_{c_{trim}} \\ \delta_e(t) - \delta_{e_{trim}} \end{bmatrix}$$

In equation error, a least-squares regression is used to identify the stability and control derivatives in $\xi$ for each force and moment coefficient, from a time history of data. As with any parameter-estimation technique, good results can only be obtained when the measured time histories for the states and controls are not highly correlated.

There are both time-domain and frequency-domain equation-error approaches. For this work, equation error in the frequency domain was used to determine stability and control derivatives. Benefits of working in the frequency domain include the ability to algebraically compute the required angular accelerations (as opposed to numerical differentiation in the time domain), increased robustness to data spikes in the measured time histories, and the ability to compute standard errors in real time. The technique used in this report, originally formulated by Morelli[7] and known as Fourier Transform Regression (FTR), utilized a recursive Fourier transform for real-time analysis as described by Morelli,[7] and was coded using MATLAB® routines from the System Identification Programs for Aircraft (SIDPAC) analysis package.[10] The recursive formulation avoided the need to store large amounts of time-history data in memory. Each recursive Fourier transform used in the FTR was a function of all the previous data in the time history being analyzed. In a real-time application, data forgetting as defined by Smith[11] could be used to delete information obtained at previous flight conditions. In this report, the forgetting was not used.

It was important to obtain the Fourier transforms at frequencies of interest to rigid body flight mechanics. For the F-15 analysis, 61 discrete frequencies were used from 0.1 Hz to 2.5 Hz at 0.04 Hz increments. Confining the data analysis to the frequency band where the system dynamics reside automatically filters out such things as the structural response modes that are typically outside of the frequency band of interest.[7]

## Output Error

For output-error PID, the vehicle system was modeled with a vector set of dynamic equations of motion. The equations of motion were derived from a general system of nine coupled nonlinear differential equations that describe the aircraft motion.[6] These equations assume a rigid vehicle and a flat, nonrotating earth. The time rate of change of mass and inertia was assumed negligible. For output-error stability and control derivative estimation, it was assumed that there is no state noise but that there is measurement (i.e., response) noise. The output-error cost function consists of a weighted least-squares measure of the agreement between the computed model response and the airplane measured response.

The F-15 configuration studied here, like most aircraft, is nearly symmetric about the *x*–*z* plane. This symmetry is used, along with small angle approximations, to simplify the coupled nonlinear equations of motion into two largely independent sets of equations describing the longitudinal and lateral-directional motions of the aircraft. Angle of attack, pitch rate, and pitch-attitude state equations were used in the longitudinal analysis. The longitudinal response equations included angle of attack, pitch rate, pitch attitude, and normal acceleration.[9] Angle of sideslip, roll rate, yaw rate, and bank-angle state equations were used in the lateral-directional analysis. The lateral-directional response equations included angle of sideslip, roll rate, yaw rate, bank angle, and lateral acceleration.[9] Use of these state and response equations enabled the estimation of all the stability and control derivatives in equations (1)–(5).

For this analysis, a time-domain output-error technique implemented in the pEst program was used.[9] An iterative approach was used to vary the stability and control derivatives until the cost function quantifying the match between model and measured outputs, as described by Murray,[9] was minimized.

The estimator also provides a measure of the reliability of each estimate based on the information obtained from each dynamic maneuver. This measure of reliability is called the Cramér-Rao bound.[6] In practice, the Cramér-Rao bound is used as a measure of relative, not absolute, accuracy.[12] A large Cramér-Rao bound indicates poor information in the data for the derivative estimate.

## MANEUVER DESIGN

Good PID maneuver design is important for accurately identifying stability and control derivatives from flight test data. A good experiment design must take into account practical constraints during the flight test while obtaining significant information content in the flight data.[6] Obtaining good information content requires exciting the system modes so that the sensitivity of the model outputs to the state and control parameters are high and correlations among the parameters are low. As stated previously, pilot inputs result in highly correlated states and controls due to the design of the control system. Therefore, a pilot-activated programmed test input that independently moved each control surface was required in order to estimate a complete stability and control derivative set.

For the IFCS application, there was an additional requirement that all the derivatives be computed as quickly as possible, which required moving all the surfaces simultaneously in a prescribed manner that would result in the desired parameter identifiability. The PreSISE were designed to meet these real-time PID objectives. The PreSISE maneuvers used stacked sine wave signals to command the control surfaces. To obtain independence, different frequencies were used for the symmetric canard, symmetric stabilator, differential canard, aileron, rudder, and differential stabilator commands. The following equation shows the control surface commands used:

$$\delta_{cmd} = A[\sin(0.625\pi B_1 t) + \sin(0.625\pi B_2 t)] \tag{12}$$

where $A$ is the amplitude and $B_1$ and $B_2$ define the frequencies at which each control surface is actuated. Table 1 shows the parameters used for this experiment.

Table 1. Parameters used to define the stacked sine wave frequencies for each control surface in the PreSISE inputs.

| Surface | $B_1$ | $B_2$ |
|---|---|---|
| Symmetric stabilator, $\delta_e$ | 1 | 3 |
| Symmetric canard, $\delta_c$ | 2 | 4 |
| Differential stabilator, $\delta_{dh}$ | 2 | 5 |
| Aileron, $\delta_a$ | 4 | 7 |
| Rudder, $\delta_r$ | 3 | 0 |
| Differential canard, $\delta_{dc}$ | 1 | 6 |

The PreSISE commands were added to the commands generated by the flight control system. The amplitude, *A*, was set the same for each surface and had values of 0.2, 0.4, and 0.8 deg, which resulted in naming the PreSISE maneuvers as small, medium, and large, respectively. The PreSISE programmed test inputs were hard coded into the flight control computer and initiated by the pilot at each test condition.

Table 2 lists three flight test conditions for this experiment. Figure 4 shows an example of a large ($A$ = 0.8°) PreSISE input at Mach 0.75 and an altitude of 20,000 ft.

Table 2. Flight test conditions.

| Test condition | Mach | Pressure altitude, ft |
|---|---|---|
| 1 | 0.75 | 20,000 |
| 2 | 0.9 | 25,000 |
| 3 | 1.2 | 32,000 |

This analysis also used pilot-input doublets. Although not all derivatives could be obtained from a doublet maneuver due to nonindependence of all controls and states, these maneuvers were still useful for evaluating results obtained from the PreSISE inputs. Typically, the pilot-input pitch doublets would generate approximately the same magnitude angle of attack, pitch rate, and normal acceleration as a large PreSISE maneuver. However, the pilot-input roll/yaw doublets would typically have larger angle of sideslip, roll and yaw rates, and lateral accelerations than the large PreSISE maneuver.

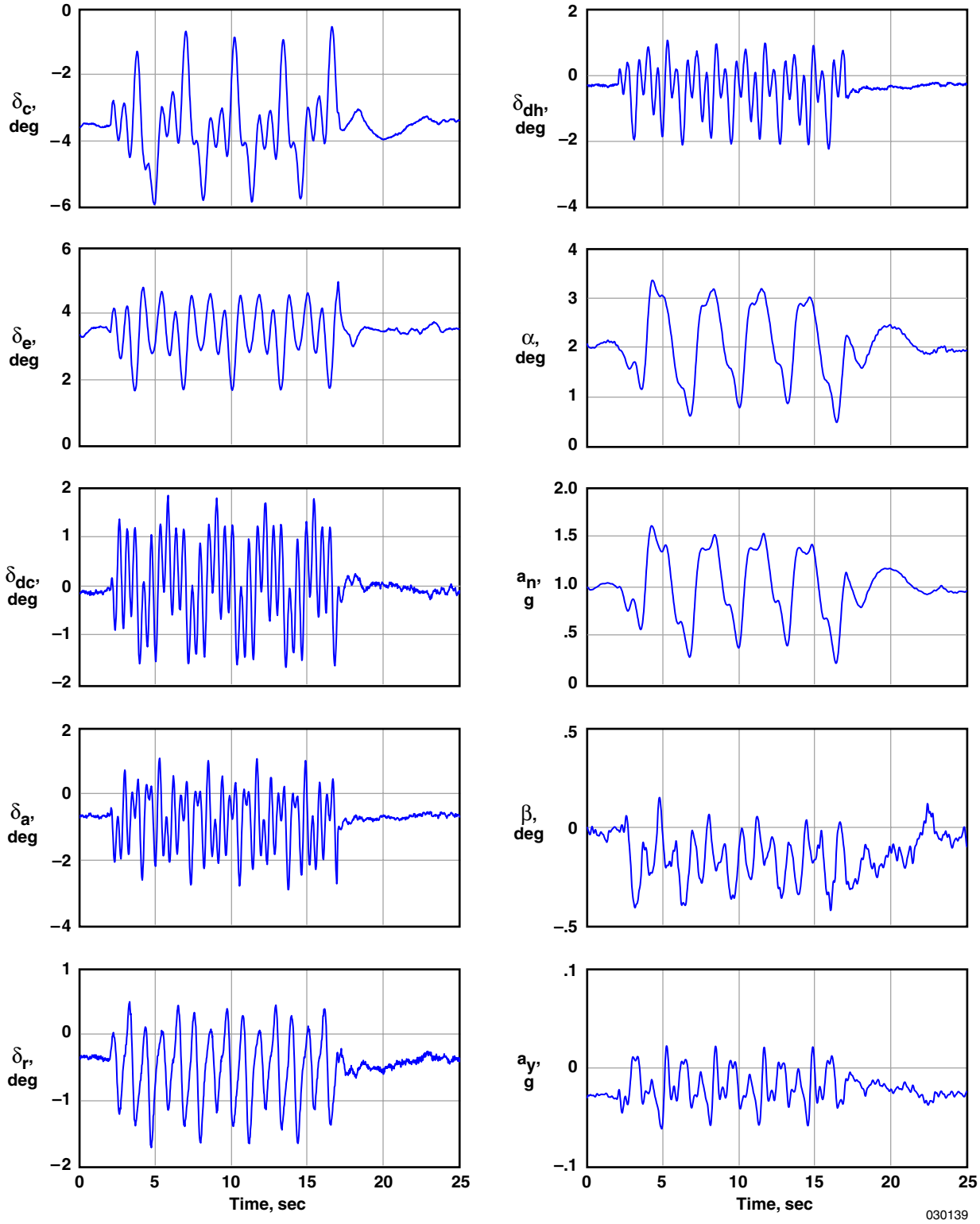


Figure 4. Time history of a large PreSISE maneuver (Mach 0.75 at 20,000 ft).

# RESULTS AND DISCUSSION

This report presents stability and control derivative results from PreSISE and doublet maneuvers. Each of the three prescribed PreSISE maneuvers were flown three times at each of the three flight test conditions, comprising a total of 27 PreSISE maneuvers that were analyzed. Also, pilot-input longitudinal and lateral-directional doublets were flown at each test condition. This section of the report will show and compare typical results from FTR and pEst analysis. For each derivative, the ordinate axis of the plot will show the range of values presented. All parameter-estimation results, including those from the real-time FTR implementation, were obtained in postflight analysis. It should be noted, however, that the FTR computation requirements were shown to be within the capabilities of the research flight computer planned to be used in a future onboard FTR implementation.[11] Also, as a means to validate the flight-estimated results, measured force and moment coefficient time histories will be compared with time histories based on estimated derivatives.

The longitudinal and lateral-directional results will be discussed separately. For pEst analysis of the PreSISE maneuvers, the longitudinal and lateral-directional equations were decoupled and analyzed separately since a formulation with all five coupled state equations showed poor results. This may have been a result of too many parameters being estimated from the data, resulting in convergence difficulties.

# LONGITUDINAL AERODYNAMICS

This section presents results from normal-force and pitching-moment coefficient derivatives. These include FTR and pEst analysis of PreSISE and doublet maneuvers.

## FTR Results

The FTR real-time equation-error technique was used to calculate all 29 stability and control derivatives listed in equations (1)–(5) from the PreSISE maneuvers. Figures 5 and 6 show longitudinal stability and control derivatives from a large amplitude ($A$ = 0.8°) PreSISE maneuver at Mach 0.75 and an altitude of 20,000 ft. Each time history includes 2 sec of data before activating the PreSISE maneuver, 15 sec of the PreSISE inputs, and 10 sec following the completion of PreSISE.

Figure 5 shows normal-force coefficient derivatives. Figure 5(a) shows the normal-force derivative due to angle of attack, $C_{N_\alpha}$. The solid line represents the FTR derivative estimate as a function of time. No prior information on estimates or standard errors were provided to the FTR technique at the start of the maneuver. The dashed line is the predicted derivative value from the linearized aerodynamic model. It was necessary to develop a scheme to identify when the FTR derivative estimates were considered valid so that they could be used by the research flight control system. The current criteria used to declare valid estimates is explained by Smith.[11] The circles in figure 5(a) indicate that the FTR code has output a derivative estimate that has been deemed valid according to the validity criteria. For the PreSISE maneuvers, the primary validity criteria was that the standard error be less than a predefined value. Table 3 shows the standard-error values used in the validity checker.

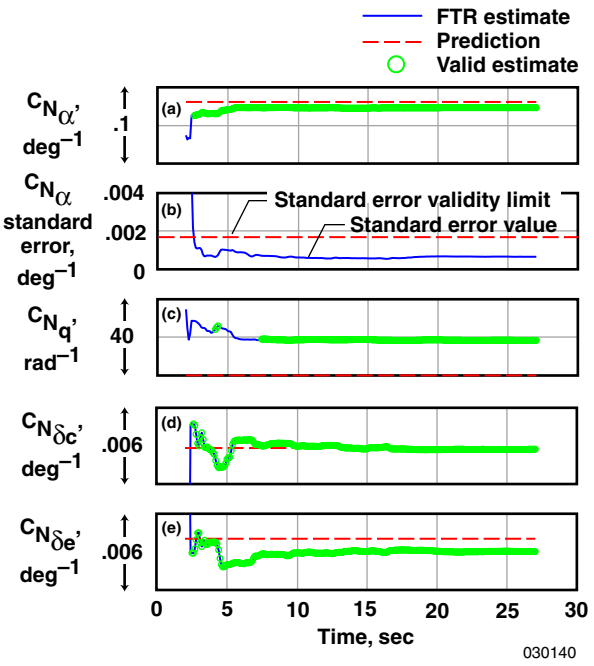


Figure 5. FTR estimates of normal-force derivatives from a large PreSISE maneuver (Mach 0.75 at 20,000 ft).

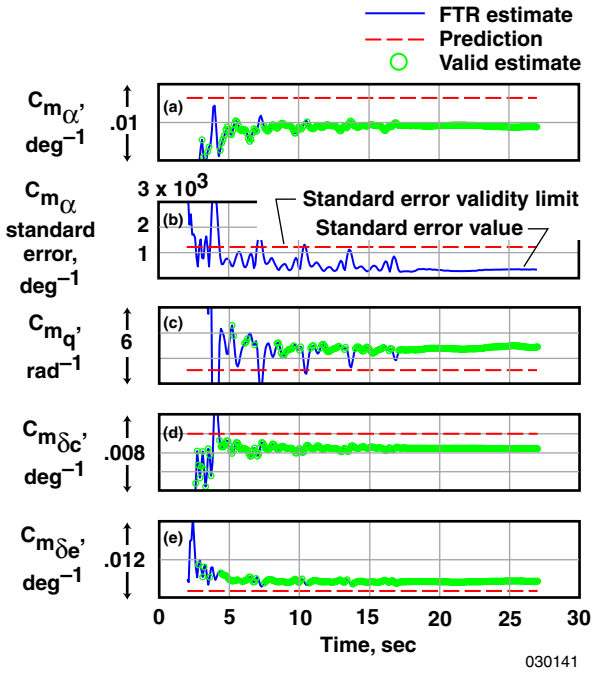


Figure 6. FTR estimates of pitching-moment derivatives from a large PreSISE maneuver (Mach 0.75 at 20,000 ft).

Table 3. Standard-error limits for the validity checker for each estimated derivative.

| | | | | | | | |
|---|---|---|---|---|---|---|---|
| $C_{N_\alpha}$ | 0.0017 deg$^{-1}$ | $C_{Y_\beta}$ | 0.0015 deg$^{-1}$ | $C_{l_\beta}$ | 0.0004 deg$^{-1}$ | $C_{n_\beta}$ | 0.0005 deg$^{-1}$ |
| $C_{N_q}$ | 1 rad$^{-1}$ | $C_{Y_p}$ | 0.1 rad$^{-1}$ | $C_{l_p}$ | 0.07 rad$^{-1}$ | $C_{n_p}$ | 0.04 rad$^{-1}$ |
| $C_{N_{\delta_c}}$ | 0.0010 deg$^{-1}$ | $C_{Y_r}$ | 0.5 rad$^{-1}$ | $C_{l_r}$ | 0.09 rad$^{-1}$ | $C_{n_r}$ | 0.15 rad$^{-1}$ |
| $C_{N_{\delta_e}}$ | 0.009 deg$^{-1}$ | $C_{Y_{\delta_r}}$ | 0.0004 deg$^{-1}$ | $C_{l_{\delta_r}}$ | 0.0002 deg$^{-1}$ | $C_{n_{\delta_r}}$ | 0.0004 deg$^{-1}$ |
| | | $C_{Y_{\delta_{dc}}}$ | 0.0004 deg$^{-1}$ | $C_{l_{\delta_{dc}}}$ | 0.0001 deg$^{-1}$ | $C_{n_{\delta_{dc}}}$ | 0.0003 deg$^{-1}$ |
| $C_{m_\alpha}$ | 0.0012 deg$^{-1}$ | $C_{Y_{\delta_a}}$ | 0.0001 deg$^{-1}$ | $C_{l_{\delta_a}}$ | 0.0001 deg$^{-1}$ | $C_{n_{\delta_a}}$ | 0.00004 deg$^{-1}$ |
| $C_{m_q}$ | 0.72 rad$^{-1}$ | $C_{Y_{\delta_{dh}}}$ | 0.0003 deg$^{-1}$ | $C_{l_{\delta_{dh}}}$ | 0.0001 deg$^{-1}$ | $C_{n_{\delta_{dh}}}$ | 0.0003 deg$^{-1}$ |
| $C_{m_{\delta_c}}$ | 0.0012 deg$^{-1}$ | | | | | | |
| $C_{m_{\delta_e}}$ | 0.0005 deg$^{-1}$ | | | | | | |

From figure 5(a), it can be seen that the converged final answer is obtained approximately 4 sec into the start of the PreSISE input. The standard-error validity checker did validate estimates before convergence. The normal-force pitch-rate derivative also converged to a final solution about 4 sec into the PreSISE maneuver (fig. 5(c)). The control derivatives (figs. 5(d) and (e)) showed that the derivatives continued to converge to the final solution throughout the PreSISE maneuver. The flight-determined normal force due to symmetric canard agreed well with the linearized aerodynamic model, whereas the normal force due to symmetric stabilator was less than predicted.

Figure 6 shows pitching-moment coefficient derivatives. Figure 6(a) shows the longitudinal stability derivative, $C_{m_\alpha}$, and figure 6(b) shows the standard-error values from the FTR $C_{m_\alpha}$ estimation. As observed in figure 6(a), the validity checker began showing valid estimates within 1 sec of the maneuver start. However, it actually took about 4 sec from the start of the PreSISE inputs for the estimates to converge near the final value. The early valid indications before actual convergence show a need for an improved validity checker. The estimates continued to change slightly during the remaining portion of the PreSISE inputs, but then achieved a steady-state value after the PreSISE inputs were completed. Similarly, the standard error reached a steady-state value after the PreSISE inputs were completed. It should be noted that for this flight condition, the flight-determined $C_{m_\alpha}$ value was significantly different than the predicted value obtained from an aerodynamic model generated primarily by wind-tunnel tests.[13] Previous flight data for this aircraft with square engine nozzles has also shown similar differences between flight and predicted $C_{m_\alpha}$.[14] Figure 6(c) shows results from the estimation of the pitching-moment damping derivative, $C_{m_q}$. The estimates varied significantly during the PreSISE inputs (as did the standard-error value that is not shown). During the PreSISE inputs, the standard-error validity checker worked well at validating estimates that were near the final value and invalidating estimates that were significantly different. Figures 6(d) and (e) show the FTR estimates of the pitching-moment effectiveness due to symmetric canards and stabilators, respectively. The estimates were similar to the $C_{m_\alpha}$ results in that the estimates converged quickly, showed slight variations during the PreSISE inputs, and maintained a steady-state value after the inputs were completed. Flight results showed lower effectiveness of the symmetric canard and symmetric stabilator than predicted.

The FTR analysis is essentially a least-squares fit of the force and moment coefficients in the frequency domain. Frequency response plots of the measured normal-force and pitching-moment coefficients were obtained at the 61 discrete frequencies used in this analysis. FTR estimated the force and moment stability and control derivatives that minimized the difference between the estimated and measured Fourier transform data for the force and moment coefficients. Figures 7 and 8 show the fits obtained using FTR for the magnitude and phase plots of normal-force and pitching-moment coefficients, respectively. As seen in figures 7 and 8, the frequency response plots show an excellent fit for magnitude at all frequencies and a very good fit of the phase angle up to 1.5 Hz. The apparent phase angle fit error at 0.46 Hz in figure 8 is simply due to the fact that the phase angle is near 180°. The phase angle fit at 0.74 Hz is not great, but it can be seen that the magnitude at that frequency is very near zero. The peaks in the magnitude plots clearly show the four frequencies at which the symmetric canard and stabilator PreSISE inputs were defined. Above 1.5 Hz, the lack of a good fit results from the fact that there were no longitudinal PreSISE inputs at those higher frequencies and therefore no usable information content in the data.

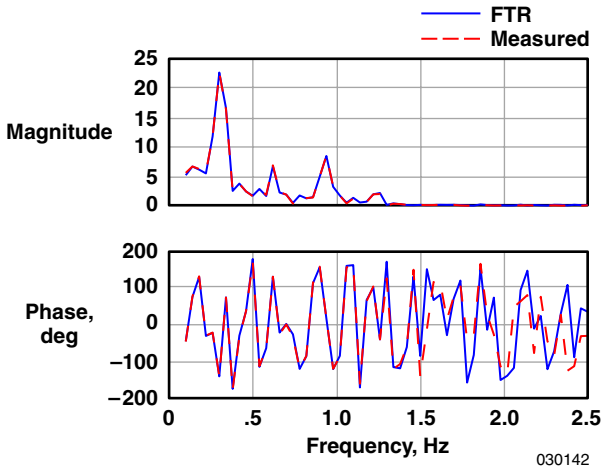


Figure 7. Normal-force coefficient frequency response from a large PreSISE maneuver (Mach 0.75 at 20,000 ft).

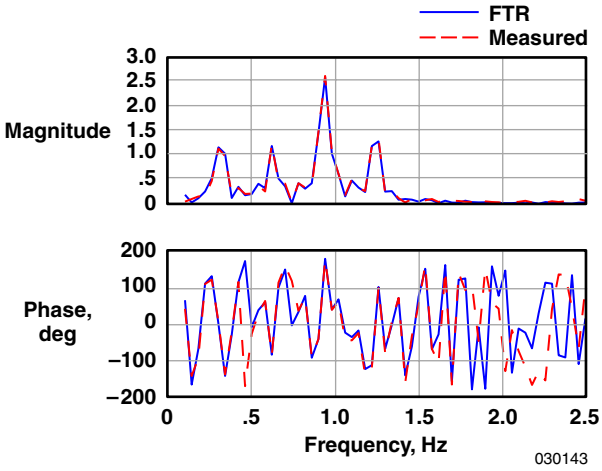


Figure 8. Pitching-moment coefficient frequency response from a large PreSISE maneuver (Mach 0.75 at 20,000 ft).

## pEst Results

The pEst output-error time-domain technique was also used to analyze the PreSISE maneuvers. In the pEst technique, the state equations of motion are integrated and the unknown stability and control parameters are changed iteratively until the estimated response time histories match the measured response time histories in a weighted least-squares sense, within the specified tolerance. For this analysis, only longitudinal equations of motion were used. Figure 9 shows the longitudinal response time histories for the same PreSISE maneuver (Mach 0.75 and an altitude of 20,000 ft) analyzed using FTR in the forementioned section. At this subsonic Mach number, the aircraft is longitudinally unstable. This required the use of pitch-rate feedback to stabilize the integrations in pEst.[15] Use of the feedback gain resulted in a solution that is a blended mix of output error and equation error with higher gains more closely representing an equation-error solution. Since the output-error solution was desired, effort was made to use the minimum amount of feedback without significantly affecting the response time histories. Typically a feedback gain of 0.4 or less was required. For figure 9, a feedback gain of 0.1 was used. Figure 9 shows excellent agreements were obtained between the estimated response time histories and the measured values.

Pilot-input doublets were also flown at the three test conditions in order to compare results with the PreSISE maneuvers. In the longitudinal axis, symmetric canard is highly correlated to angle of attack. Therefore, symmetric canard derivatives were not estimated in the pEst analysis. Solutions from pEst were obtained in two ways. In one case, the canard derivatives were set equal to predicted aerodynamic model values from the wind-tunnel data in the simulation. In a second case, the canard derivatives were set to the values estimated from pEst analysis of the PreSISE maneuvers. Excellent agreement was obtained between the measured response time histories and the pEst time histories for both cases. Figure 10 shows this agreement for a doublet flown at Mach 0.75 and an altitude of 20,000 ft with the symmetric canard values set equal to the value obtained from the pEst analysis of the PreSISE maneuvers. In general, the fit is excellent. The worst fit is for angle of attack. Of the four longitudinal response parameters, however, angle of attack is the most difficult to measure and therefore has a reduced weighting in the pEst analysis.

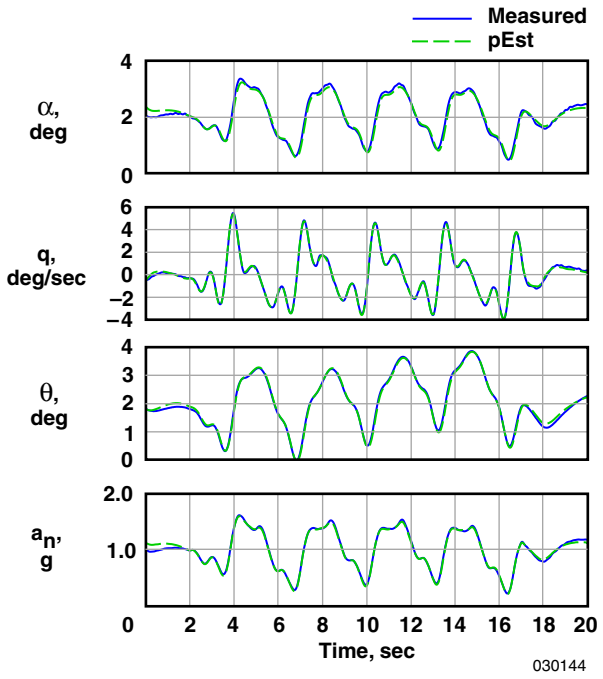


Figure 9. Response time histories using pEst for a large PreSISE maneuver (Mach 0.75 at 20,000 ft).

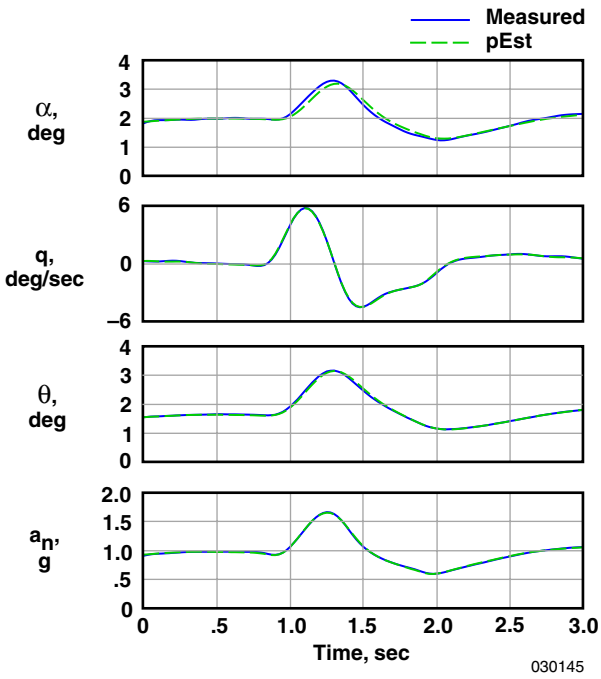


Figure 10. Response time histories using pEst for a pilot-input longitudinal doublet maneuver (Mach 0.75 at 20,000 ft).

## Comparison of FTR and pEst Results

Figures 11 and 12 show normal-force and pitching-moment derivative results from FTR and pEst analysis of PreSISE and doublet maneuvers for the test condition of Mach 0.75 and an altitude of 20,000 ft. At this test condition, three each of the small, medium, and large PreSISE inputs and three pilot-input pitch doublets were flown. In figures 11 and 12, the small, medium, and large PreSISE inputs and the doublets are grouped separately for easy comparison. All moment derivatives shown in figure 12 are referenced to the aerodynamic model moment reference (25.65-percent reference chord). The FTR results were obtained by averaging all the valid FTR outputs from the maneuver. The recursive FTR analysis generated outputs at 10 Hz. The error bars on the FTR results represent the calculated standard error, and the error bars on the pEst results were determined by multiplying the Cramér-Rao bounds by a factor of five.[6]

Figure 11 shows the normal-force derivatives. The circle symbols represent the FTR analysis of the PreSISE maneuvers and the asterisk symbols represent the pEst analysis of the PreSISE maneuvers. Figure 11(a) shows the symmetric canard derivative estimate. This derivative was only estimated from the PreSISE maneuvers. FTR and pEst analysis showed the $C_{N_{\delta_c}}$ estimates very near the predicted value with some scatter. The scatter was minimal for the large PreSISE maneuvers (with the exception of the pEst result from the first of the three maneuvers). Since the derivative estimated from the PreSISE maneuvers agreed with the prediction, the doublet analysis using pEst was only done using the predicted $C_{N_{\delta_c}}$ derivative. The square symbols shown in figures 11(b–d) are results from the pEst analysis of the doublet maneuvers using the aerodynamic model prediction of $C_{N_{\delta_c}}$ for the analysis.

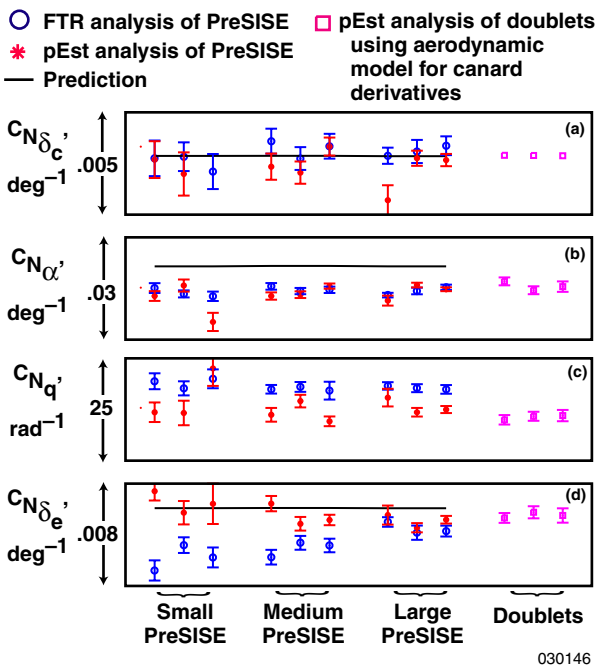


Figure 11. FTR and pEst normal-force derivative estimates (Mach 0.75 at 20,000 ft).

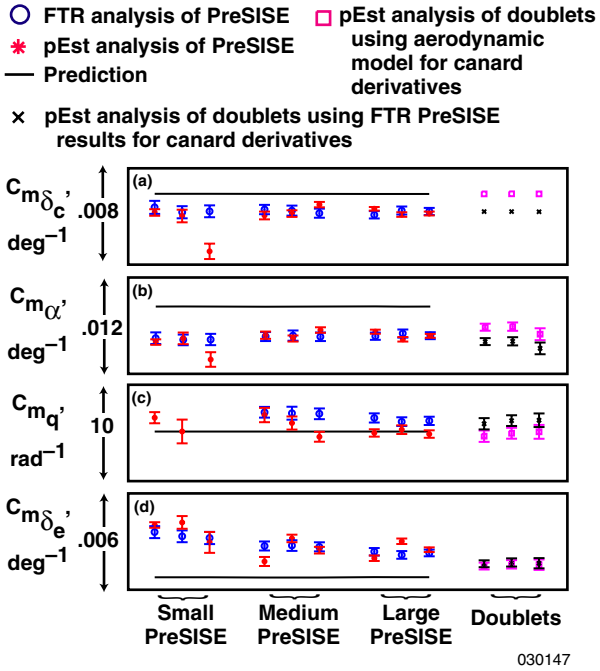


Figure 12. FTR and pEst pitching-moment derivative estimates (Mach 0.75 at 20,000 ft).

Figure 11(b) shows good agreement exists between the FTR and pEst estimates of the normal-force angle-of-attack derivative from PreSISE maneuvers. The size of the maneuver did not significantly affect the results, although standard errors are slightly smaller for the large PreSISE maneuvers. The doublet analysis agreed with the analysis from the PreSISE maneuvers. The pitch-rate derivative, $C_{N_q}$, in figure 11(c) shows a difference between FTR and pEst analysis of the PreSISE maneuvers. The standard errors became generally smaller with the larger PreSISE inputs. Figure 11(d) shows the symmetric stabilator derivative results. For this case, the size of the PreSISE inputs affected the derivative estimates. The large PreSISE inputs agreed well with the pEst results and generally had smaller standard errors. The doublet analysis also showed results consistent with the large PreSISE maneuvers.

Figure 12 shows the pitching-moment derivatives. Figure 12(a) shows the pitching moment due to symmetric canard. FTR and pEst results of the PreSISE maneuvers agreed well, independent of the size of the maneuver. These results showed lower pitching-moment effectiveness than predicted. Consequently, the pEst analysis of the doublets was done using the predicted $C_{m_{\delta_c}}$ values represented by the square symbols and the $C_{m_{\delta_c}}$ values estimated from the PreSISE maneuvers represented by

the *x* symbols. Figure 12(b) shows the estimated longitudinal stability derivative, $C_{m_\alpha}$. At this flight condition, the $C_{m_\alpha}$ values are positive since the airplane is longitudinally unstable. FTR and pEst analysis of the PreSISE maneuvers show excellent agreement in estimating $C_{m_\alpha}$ and show a value significantly less than predicted. The analysis of the doublet maneuvers shows good agreement with the PreSISE results, although the pEst analysis of the doublets using the estimate of the $C_{m_\delta}$ from the PreSISE maneuvers (*x* symbols) is noticeably less than the FTR estimated $C_{m_\alpha}$ (circle symbols). Figure 12(c) shows the pitch damping derivative, $C_{m_q}$. For this derivative, the large PreSISE maneuvers showed good agreement with the predicted value (especially using the pEst analysis). FTR results for the small maneuver are not shown since the results never passed the validity checker. The results from the pitch doublets agreed well with the results from the large PreSISE maneuvers. Figure 12(d) shows the symmetric stabilator pitch effectiveness results. The size of the PreSISE maneuver does affect the estimate for both FTR and pEst analysis. Although absolute derivative values are not shown in the plots, the results from the doublets and large PreSISE maneuvers agree reasonably well with each other and the prediction. The doublets, however, consistently show slightly more stabilator pitching-moment effectiveness than estimated from the PreSISE maneuvers.

Figure 13 shows data results for $C_{m_\alpha}$ for Mach 0.9 and an altitude of 25,000 ft, and in figure 14 for Mach 1.2 and an altitude of 32,000 ft. It is clearly evident in figure 14 that using the symmetric canard derivatives obtained from the PreSISE maneuvers in the pEst analysis of the doublets results in better agreement with $C_{m_\alpha}$ derivative pEst estimates from PreSISE maneuvers.

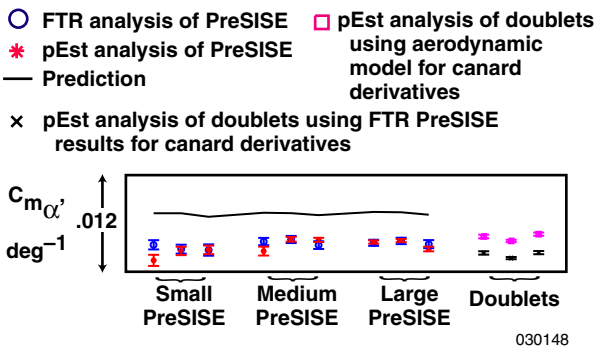


Figure 13. FTR and pEst estimates (Mach 0.90 at 25,000 ft).

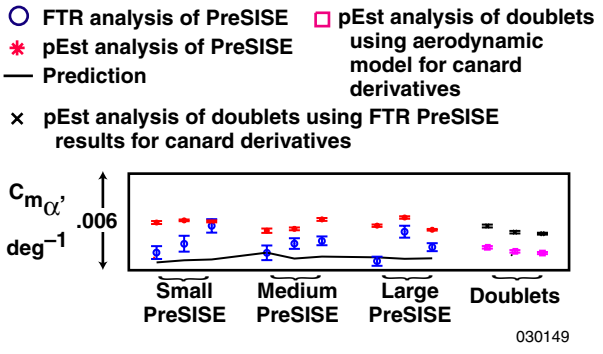


Figure 14. FTR and pEst estimates (Mach 1.20 at 32,000 ft).

## Evaluation Maneuver

A pilot-input pitch-doublet maneuver was used to assess the accuracy of the parameter-estimation results. Figure 15 shows results from a pitch-doublet maneuver at Mach 0.75 and an altitude of 20,000 ft that was not used in determining derivative estimates. For this analysis, the estimated longitudinal stability and control derivatives were used in equations (1) and (2) to obtain normal-force and pitching-moment coefficients, respectively. These values were then compared with the measured coefficient values obtained from equations (6) and (7). To compare results, the trim values were removed as the bias terms in equations (1) and (2) were not estimated in the PID analysis. Figure 15(a) shows the normal-force coefficient and figure 15(b) shows the pitching-moment coefficient. The solid line represents the measured value, the dashed line is the coefficient time histories using the derivatives estimated from FTR analysis of the large PreSISE maneuvers, and the dash-dot line was obtained using the preflight predicted aerodynamic model for the aircraft (coefficient time histories representing the pEst analysis of PreSISE and doublet maneuvers are not shown in order to simplify the plots, but agree well with the time histories from the FTR analysis). The normal-force coefficient plots in figure 15(a) show good agreement between the measured and FTR estimated coefficient. The predicted aerodynamic model did show slight overshoots during the doublet maneuver. The pitching-moment coefficient plots in figure 15(b) also show very good agreement between the measured and FTR estimated value. Again, the predicted aerodynamic model shows the most error when compared with the measured value indicating that the FTR analysis of the PreSISE maneuvers resulted in improved longitudinal derivatives as compared to the predicted values. Recall from figures 5 and 6 that there were some significant differences between the predicted and estimated longitudinal stability and control derivatives. Figure 15 demonstrates the adequacy of the FTR PID approach to obtaining longitudinal derivatives from the large PreSISE maneuvers. The medium and small PreSISE maneuvers were less successful, but still gave reasonably good results, as evidenced from the comparisons in figures 11 and 12.

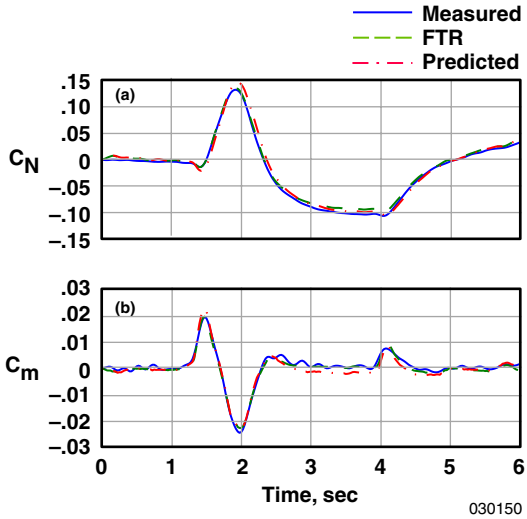


Figure 15. Longitudinal force and moment coefficients from a doublet maneuver (Mach 0.75 at 20,000 ft).

## LATERAL-DIRECTIONAL AERODYNAMICS

This section presents results from side-force, rolling-moment, and yawing-moment coefficient derivatives. These include FTR and pEst analysis of PreSISE and doublet maneuvers.

### FTR Results

Figures 16–18 show lateral-directional stability and control derivatives from a large amplitude PreSISE maneuver at Mach 0.75 and an altitude of 20,000 ft. These results are from the same PreSISE maneuver analyzed in the previous longitudinal aerodynamics section. Each time history includes 2 sec of data before activating the PreSISE maneuver, 15 sec of the PreSISE inputs, and 10 sec following the completion of PreSISE.

Figure 16 shows the FTR estimated side-force derivatives. All the derivative estimates converged to a validated solution within approximately 5 sec of the start of the PreSISE inputs. Figure 17 shows the rolling-moment derivatives. The dihedral effect parameter, $C_{l_\beta}$, in figure 17(a) converged within approximately 3 sec of starting the PreSISE inputs. As in the longitudinal cases, the derivative estimate varies slightly during the 15 sec PreSISE input before achieving a steady-state value after the inputs are complete. In this case, the final value did drift slightly and showed a less negative value than predicted. Figures 17(b) and (c) show fairly rapid convergence of the dynamic derivatives; however, the current validity checker did not validate the $C_{l_r}$ estimate except for a few early estimates which were not the converged answer. This lack of validation again highlights a need to improve the accuracy and robustness of the validity criteria. The rolling-moment control derivatives all converged rapidly (figs. 17(d–g)) with the rudder derivative showing the most variation during the PreSISE inputs. The estimates showed that the rudder effectiveness was predicted well by the aerodynamic model, whereas the effectiveness of differential canard, aileron, and differential stabilator were all slightly underpredicted.

Figure 18 shows the yawing-moment derivatives. The directional stability derivative, $C_{n_\beta}$, in figure 18(a) converged rapidly to the predicted level. Figure 18(b) shows the yawing moment due to roll-rate derivative estimate drift during the PreSISE inputs to a steady-state value after the inputs were completed. The yawing-moment control derivatives shown in figures 18(d–g) all converged to a validated solution. The most significant control derivative, $C_{n_{\delta_r}}$, showed slightly less effectiveness than predicted.

Frequency response plots of the measured side-force, rolling-moment, and yawing-moment coefficients were obtained at the 61 discrete frequencies used in this analysis. Figures 19–21 show the frequency response plots from measured and FTR estimated side-force and rolling- and yawing-moment coefficients. The frequency response plots for side force in figure 19 show an excellent fit of the magnitude at all frequencies, with the small exception near 1.9 Hz. The phase angle plots show good fits up to approximately 1.7 Hz (the apparent problem near 0.4 Hz is due to plotting values near ±180°). The frequency response plots for rolling moment in figure 20 are good, but problems exist at the lower frequencies. Good fits are achieved at frequencies corresponding to aileron and differential stabilator that are the primary roll effectors. The magnitude fit for the yawing-moment frequency response plot in figure 21 is excellent, but there are problems with the phase angle plots at frequencies below 0.5 Hz and above 1.9 Hz. The best fit of the yawing-moment frequency response occurs at approximately 0.94 Hz that corresponds to the rudder input, which is the primary yaw effector.

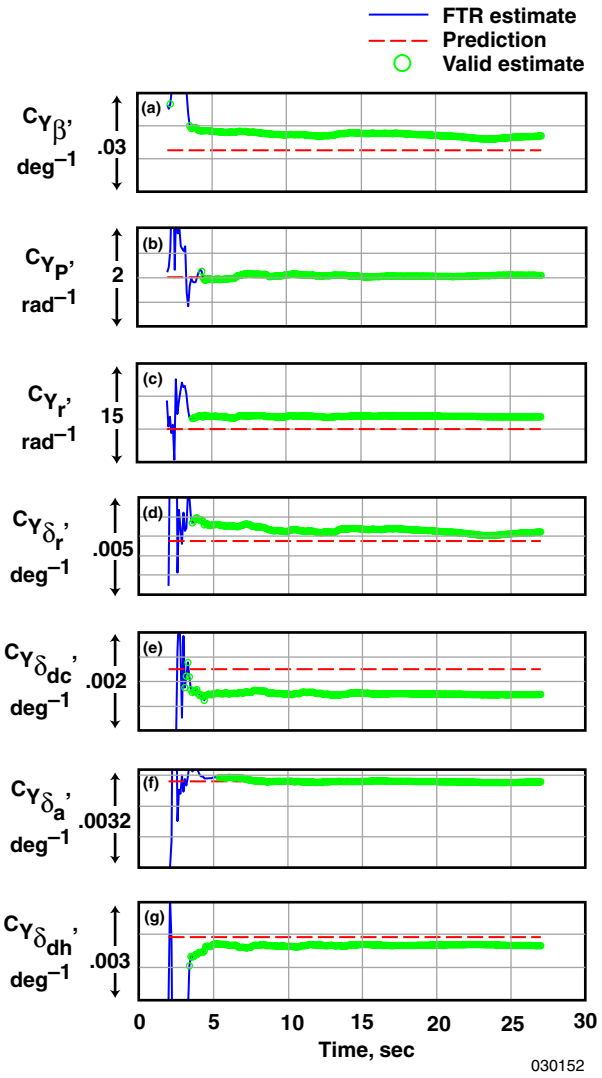


Figure 16. FTR estimates of side-force derivatives from a large PreSISE maneuver (Mach 0.75 at 20,000 ft).

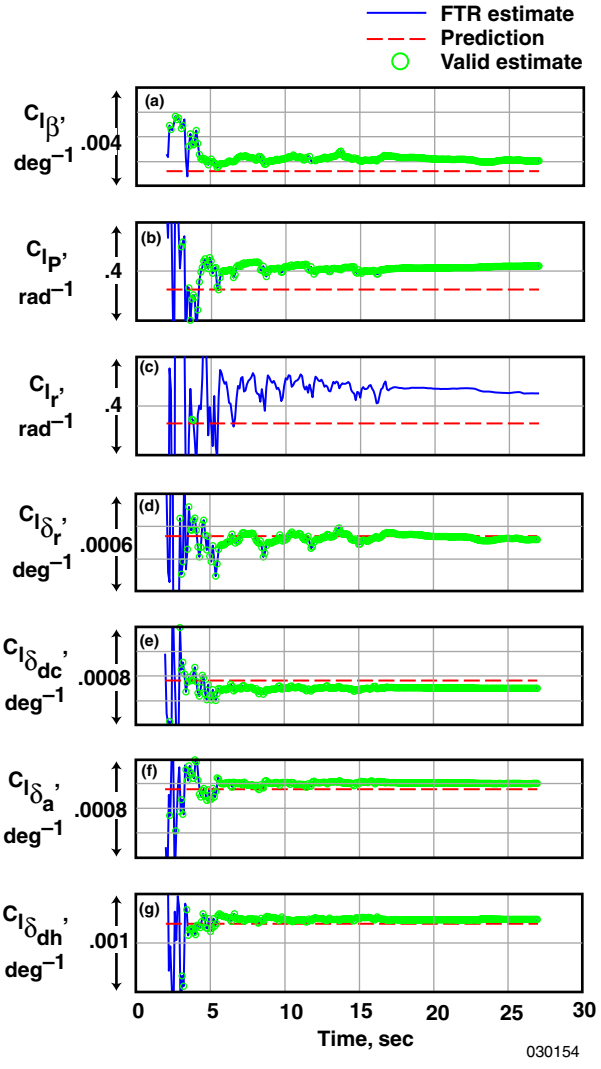


Figure 17. FTR estimates of rolling-moment derivatives from a large PreSISE maneuver (Mach 0.75 at 20,000 ft).

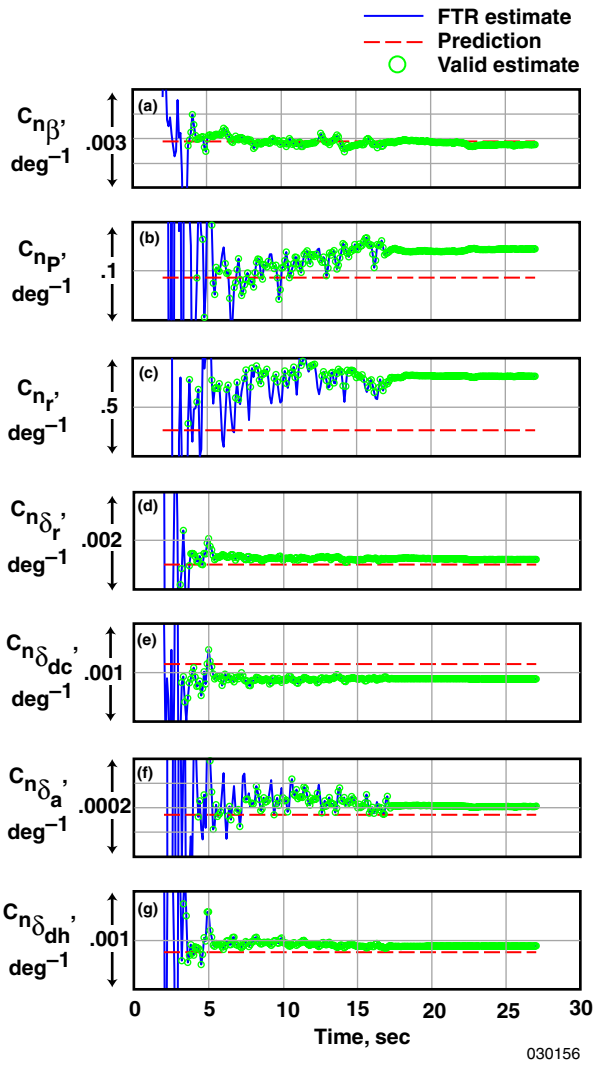


Figure 18. FTR estimates of yawing-moment derivatives from a large PreSISE maneuver (Mach 0.75 at 20,000 ft).

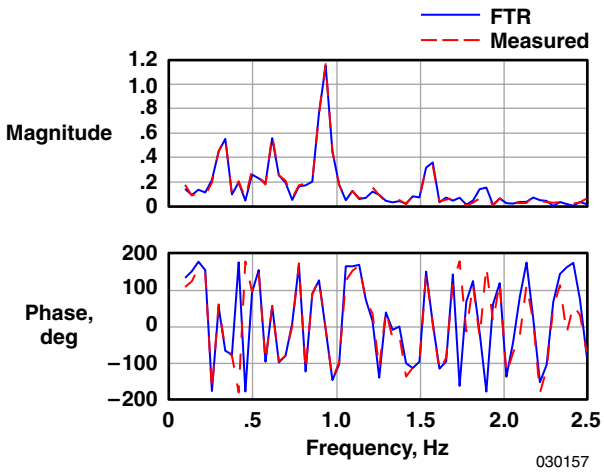


Figure 19. Side-force coefficient frequency response from a large PreSISE maneuver (Mach 0.75 at 20,000 ft).

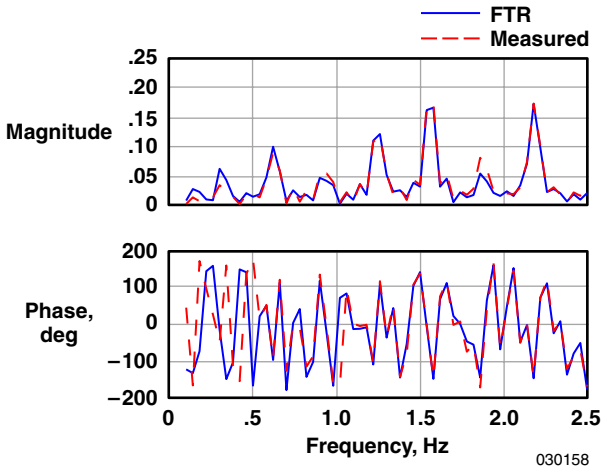


Figure 20. Rolling-moment coefficient frequency response from a large PreSISE maneuver (Mach 0.75 at 20,000 ft).

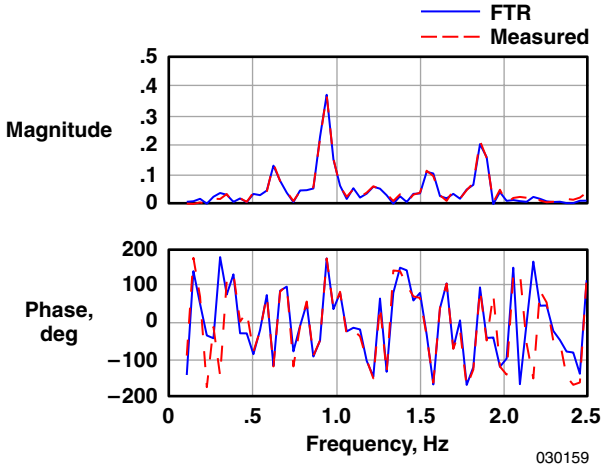


Figure 21. Yawing-moment coefficient frequency response from a large PreSISE maneuver (Mach 0.75 at 20,000 ft).

## pEst Results

As done previously for the longitudinal analysis, pEst was also used to analyze lateral-directional aerodynamics from the PreSISE maneuvers. For this analysis, only lateral-direction equations of motion were used. Figure 22 shows the lateral-directional response time histories for the same PreSISE maneuver (Mach 0.75 and an altitude of 20,000 ft) analyzed using FTR. Unlike the longitudinal pEst response time histories in figure 9, the lateral-directional analysis does not show good agreements between the estimated and measured response time histories. The yaw rate fit is very good; however, the very important lateral acceleration fit is very poor.

This poor fit may be a result of the fact that significant longitudinal motions were a part of the PreSISE maneuvers. Using a coupled longitudinal and lateral-directional pEst analysis did not improve the results. Consequently, this report will not present lateral-directional pEst results from the PreSISE maneuvers. Pilot-input lateral-directional doublet maneuvers, however, were successfully analyzed with pEst to compare with the FTR analysis of the PreSISE maneuvers. As stated previously, in the lateral-directional axes, aileron and differential stabilator were highly correlated as were rudder and differential canard. In the doublet analysis, it was chosen not to estimate aileron and differential canard derivatives. As in the longitudinal analysis, solutions from the pEst doublet analysis were obtained in two ways. In one technique, the aileron and differential canard derivatives were set equal to aerodynamic model values. In the second technique, the aileron and differential canard derivatives were set to the values predicted by FTR analysis of the PreSISE maneuvers. Excellent agreement was obtained between the measured response time histories and the measured pEst time histories using both techniques. Figure 23 shows this agreement for a doublet flown at Mach 0.75 and an altitude of 20,000 ft with the aileron and canard values set equal to the value obtained from the PreSISE FTR analysis. A comparison of figures 22 and 23 shows that the aircraft responses to the doublets are considerably larger and lower frequency than the responses to the large PreSISE maneuver. These slower, larger responses and the prior information on some of the parameters are likely reasons that the pEst fits were better for the doublet maneuvers.

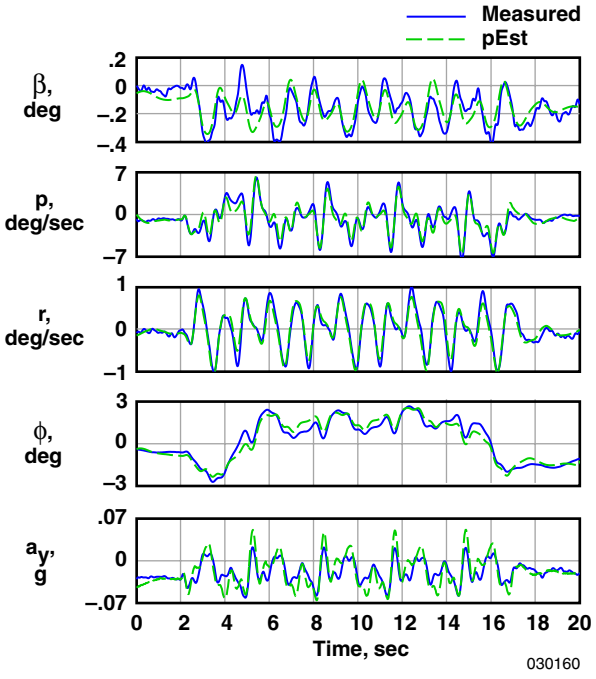


Figure 22. Lateral-directional response time histories using pEst for a large PreSISE maneuver (Mach 0.75 at 20,000 ft).

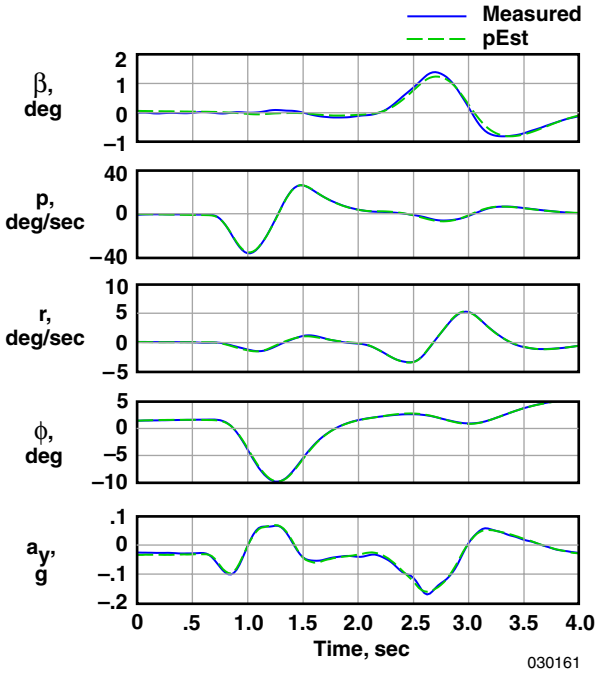


Figure 23. Lateral-directional response time histories using pEst for a pilot-input doublet maneuver (Mach 0.75 at 20,000 ft).

## Comparison of FTR PreSISE and pEst Doublet Results

Figures 24–26 show side-force and rolling- and yawing-moment derivative results from FTR analysis of the PreSISE maneuvers and pEst analysis of doublet maneuvers for the test condition of Mach 0.75 and an altitude of 20,000 ft. Three each of the small, medium, and larger PreSISE inputs and three pilot-input pitch doublets were analyzed. All moment derivatives in figures 25 and 26 are referenced to the aerodynamic model moment reference.

Figure 24 shows the side-force derivatives. The circle symbols represent the FTR analysis of the PreSISE maneuvers. In general, the FTR analysis showed consistent results irrespective of the size of the inputs for each of the estimated derivatives. The FTR estimates of $C_{Y_{\delta_\alpha}}$ (fig. 24(b)) were only considered valid for the large PreSISE maneuvers due to large standard errors. The aileron, rudder, and differential stabilator derivative estimates showed good agreement with predictions. The pEst analysis of the doublet maneuvers generally confirmed the FTR results. The use of the FTR-determined differential canard derivative in the pEst analysis brought the rudder derivative estimate into better agreement with the FTR results from the PreSISE maneuvers (fig. 24(f)).

Figure 25 shows the rolling-moment derivative estimates. The size of the PreSISE maneuver did affect the FTR results as can be clearly seen in the aileron and differential stabilator derivative estimates. In the case of the aileron derivatives, valid FTR estimates were only obtained from the large PreSISE maneuvers (fig. 25(b)). The pEst analysis of the doublet maneuvers showed good repeatability and typically good agreement with the predicted derivatives, with the exception of the rudder derivative (fig. 25(f)). Use of the FTR estimates of differential canard and aileron derivatives in the pEst analysis of the doublet maneuver did not result in improved agreement with the FTR estimated rudder derivative (fig. 25(f)).

Figure 26 shows the yawing-moment derivative estimates. The FTR analysis of the PreSISE maneuvers showed significantly different $C_{n_{\delta_{dc}}}$ and $C_{n_{\delta_a}}$ estimates compared with the predictions (figs. 26(a) and (b)). The FTR estimate of $C_{n_\beta}$ showed similar results irrespective of the maneuver size and agreed reasonably well with the prediction (fig. 26(c)). The pEst analysis of the doublet maneuvers showed some interesting results. The sideslip and rate derivatives showed results that agreed reasonably well with the FTR results and the predictions. The control derivative estimates, however, showed significantly different results depending on whether the predicted or FTR-determined estimates of differential canard and aileron derivatives were used. Figure 26(f) shows that the rudder derivative estimated using pEst with predicted $\delta_a$ and $\delta_{dc}$ derivatives agreed much better with FTR PreSISE results than using $\delta_a$ and $\delta_{dc}$ derivatives from FTR analysis. Similar results were seen for $C_{n_{\delta_{dh}}}$ estimates from the doublet maneuvers. These large differences cast doubts on the usability of the PreSISE maneuvers in estimating accurate yawing-moment derivatives.

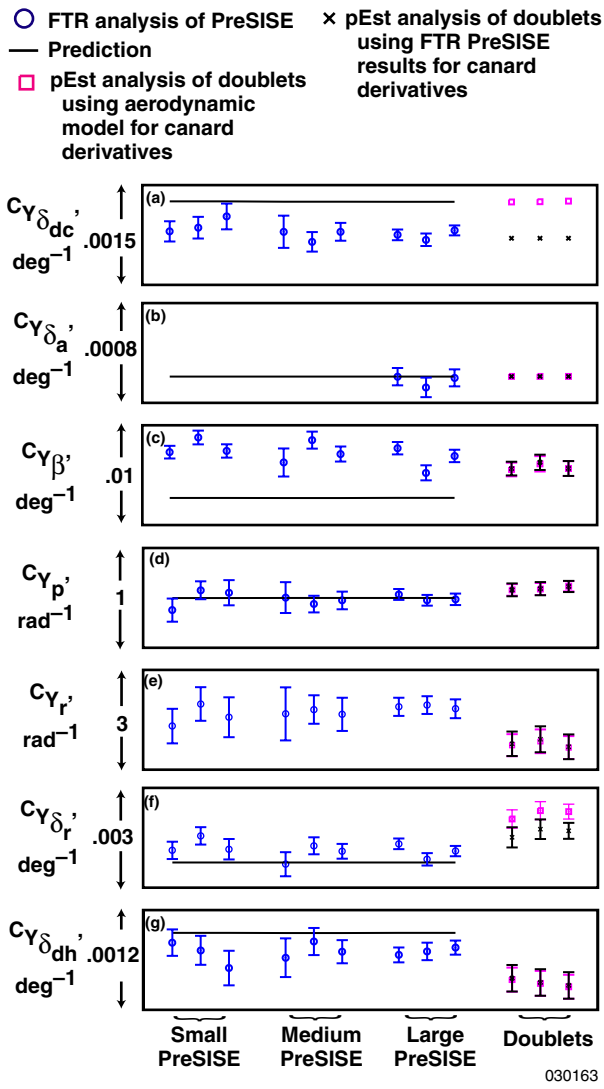


Figure 24. FTR and pEst side-force derivative estimates (Mach 0.75 at 20,000 ft).

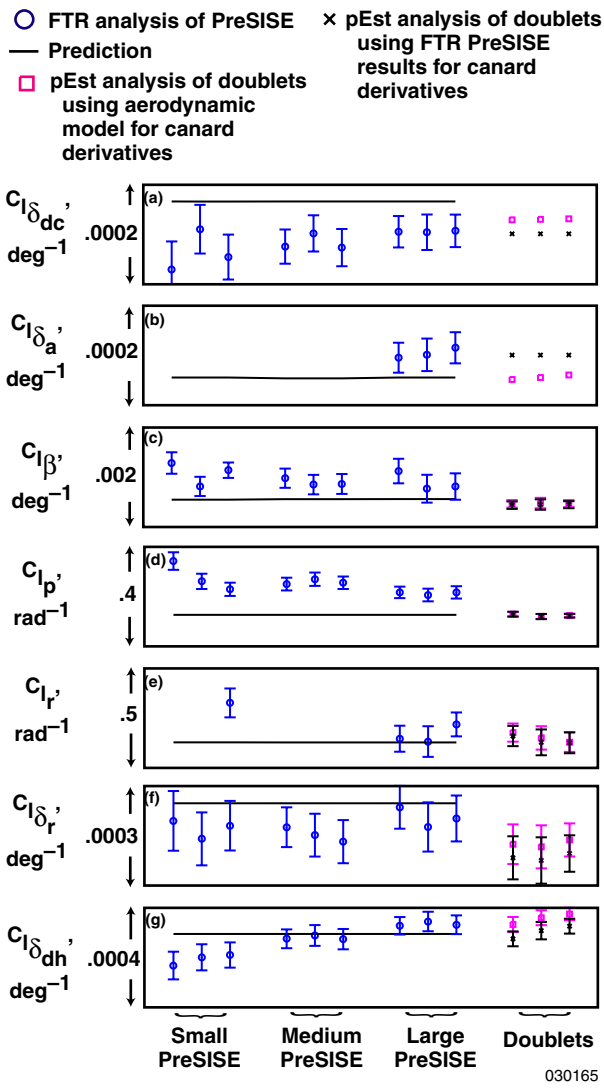


Figure 25. FTR and pEst rolling-moment derivative estimates (Mach 0.75 at 20,000 ft).

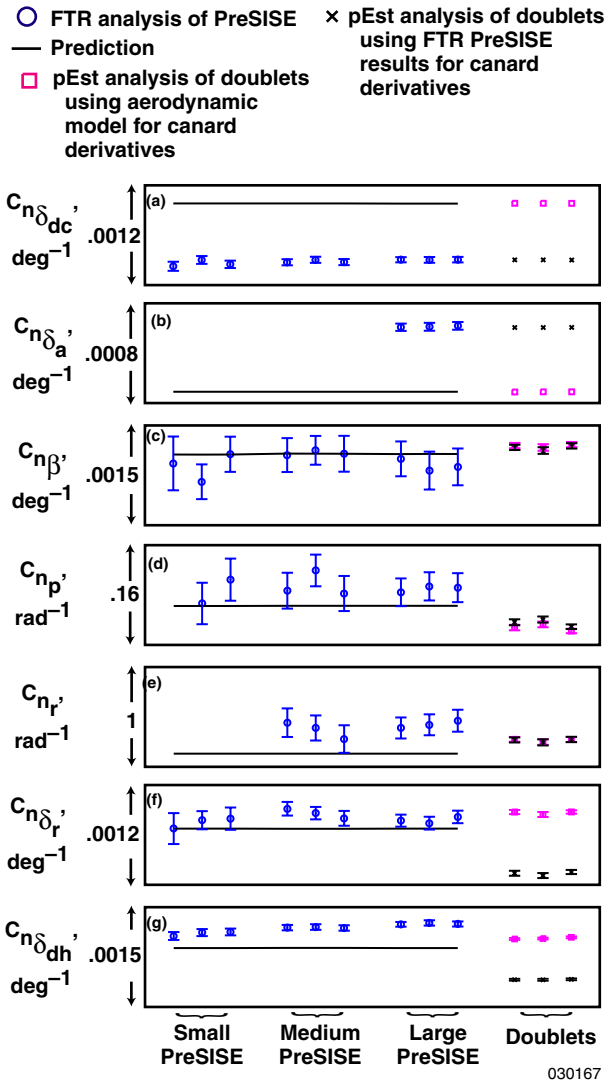


Figure 26. FTR and pEst yawing-moment derivative estimates (Mach 0.75 at 20,000 ft).

## Comparison With Flight Data

A pilot-input yaw/roll doublet maneuver was used to assess the accuracy of the parameter-estimation results. Figure 27 shows results from a yaw doublet immediately followed by a roll doublet at Mach 0.75 and an altitude of 20,000 ft. This particular maneuver was not used in determining derivative estimates. Estimated lateral-directional stability and control derivatives were used in equations (3)–(5) to obtain side-force, rolling-moment, and yawing-moment coefficients, respectively. These values were then compared with the measured coefficient values obtained from equations (8)–(10). To compare results, the trim values were removed as the bias terms in equations (3)–(5) were not estimated in the PID analysis. The solid line in figure 27 represents the measured value, the dashed line is the coefficient estimates using the derivatives estimated from FTR analysis of the large PreSISE maneuvers, the dash-dot line is the coefficient estimates using the derivatives estimated from pEst analysis of the doublet maneuvers with aerodynamic model predictions for the nonestimated differential canard and aileron derivatives, and the dash-dot-dot line was obtained using the preflight predicted aerodynamic model for the aircraft. Figure 27(a) shows the side-force coefficient plots. Good agreement is seen between the measured and estimated coefficient time histories. Figure 27(b) shows the rolling-moment coefficient plots. In this case, the largest errors are for the time histories based on FTR analysis of the PreSISE maneuvers. The time history resulting from pEst analysis of the doublet maneuvers resulted in good agreement with the measured time history. Figure 27(c) shows the yawing-moment coefficient plots. The largest errors were again related to the FTR analysis of the PreSISE maneuvers. The pEst analysis of the doublet maneuvers resulted in time histories that agreed well with the measured time history. In general, figure 27 indicates inaccuracies in the FTR analysis of the PreSISE maneuvers. It is concluded that the PreSISE maneuvers are not adequate for accurate lateral-directional derivative estimation. Uncertainty exists regarding the actual problem, but it could be that the amplitude of the maneuvers was too small or the frequency content was too little or both occurred. Morelli[16] has proposed an optimization scheme to improve the PreSISE input for better stability and control derivative estimation without requiring larger amplitude inputs. Future flight tests are required to validate this technique.

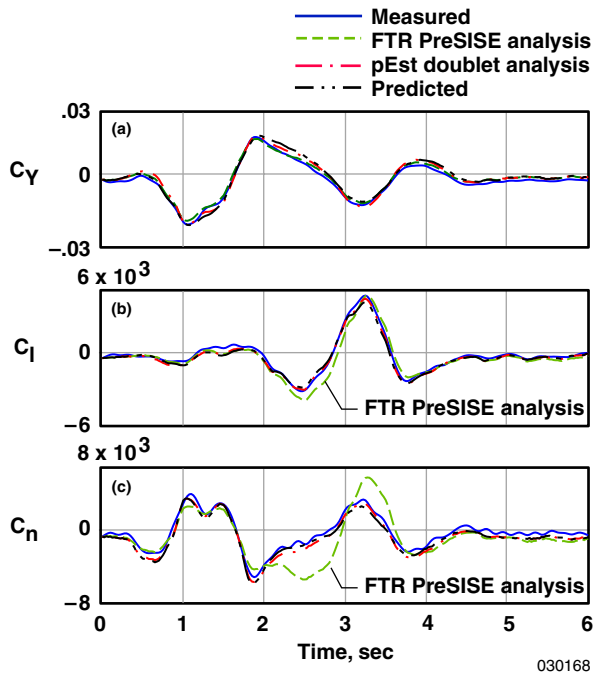


Figure 27. Lateral-directional force and moment coefficients from a doublet maneuver (Mach 0.75 at 20,000 ft).

# CONCLUDING REMARKS

Near real-time onboard stability and control derivative extraction is required to support the flight demonstration of an Intelligent Flight Control System (IFCS) concept developed by NASA, academia, and industry. The goal of the IFCS program is the ability to modify in real time the control laws for an aircraft that has been damaged in flight (such as battle damage, weather, or system failure). Initial flight tests have been conducted to assess the accuracy and robustness of a proposed onboard real-time implementation of a stability and control parameter identification technique. A new control-surface excitation technique known as Prescribed Simultaneous Independent Surface Excitation (PreSISE) was utilized for this study to accommodate the real-time requirements. The PreSISE maneuver consisted of the flight computer commanding all surfaces simultaneously with sinusoidal motions at unique frequencies for each control surface to reduce correlations between control surfaces and aircraft states. These correlations can be high for pilot-input maneuvers as a result of actions of the control system.

This report presents results from flight tests of the PreSISE inputs and from pilot-input doublet maneuvers. Tests were conducted at subsonic, transonic, and supersonic conditions. Both equation-error and output-error parameter-estimation techniques were utilized to obtain aerodynamic stability and control derivatives from the maneuvers. The equation-error technique, known as Fourier Transform Regression (FTR), estimates derivatives in the frequency domain and was developed for future on-aircraft real-time implementation. The output-error technique, known as pEst, estimates derivatives in the time domain and was run in a postflight batch mode.

Longitudinal aerodynamic analysis included estimating normal-force and pitching-moment derivatives. The FTR analysis of the PreSISE maneuvers was shown to converge rapidly (usually within 5 sec) and accurately when compared to pEst results using both PreSISE and doublet maneuvers. Three different amplitudes of surface excitations were tested using the PreSISE technique. For some derivatives, the smaller amplitude maneuvers were not adequate for accurate identification. Because of a high correlation between angle of attack and symmetric canard, the symmetric canard derivative was not estimated from the doublet maneuvers. Using the PreSISE-determined canard derivatives in the pEst doublet analysis, however, resulted in generally good agreement between PreSISE and doublet derivative estimation and especially at the supersonic test condition. Comparison of normal-force and pitching-moment coefficient time histories using estimated derivatives with the flight-measured coefficient time histories was excellent and showed a slight improvement over using the predicted aerodynamic model derivatives. This demonstrated good accuracy of the longitudinal FTR analysis of the large PreSISE maneuvers.

Use of the PreSISE maneuvers for lateral-directional stability and control derivative estimation was less effective than the longitudinal analysis. In the lateral-directional axes, side-force, rolling-moment, and yawing-moment derivatives were estimated from flight data. In general, the FTR analysis was able to obtain a converged solution from the PreSISE maneuvers. The larger maneuvers would typically result in quicker (and more accurate) convergence. The pEst analysis, however, showed that it was difficult to get good fits of the response time histories from the PreSISE maneuvers; and therefore, pEst results were not used in this analysis. It was suspected that the poor fits in the pEst analysis of the PreSISE maneuvers were a result of small aircraft responses with consequent low data information content and possibly coupled longitudinal inputs in the maneuver. The pEst analysis, however, was useful for analyzing pilot-input doublet maneuvers. Results from the doublets were very consistent among multiple maneuvers. In the lateral-directional axes, the aileron and differential stabilator were highly correlated as

were the rudder and differential canard. Consequently, differential canard and aileron derivatives were not estimated from the pilot-input doublet maneuvers. Use of the PreSISE-estimated differential canard and aileron derivatives to improve the doublet analysis was only successful for a few derivatives. Comparison of side-force, rolling-moment, and yawing-moment coefficient time histories from estimated derivatives with the flight measured coefficient time histories showed decent results, but also demonstrated inaccuracies in the FTR analysis of the PreSISE maneuvers.

In summary, the PreSISE inputs in combination with FTR shows promise for obtaining rapid estimates of aerodynamic stability and control derivatives from onboard real-time processing. With the defined PreSISE maneuvers, estimates of longitudinal derivatives from the FTR technique were in very good agreement with estimates from pEst. For the lateral-directional cases, difficulties in estimating accurate parameters using FTR and pEst suggests that the data information content for the lateral-directional maneuvers was insufficient. Additional work is required to better define the maneuvers for accurate estimation of lateral-directional derivatives.

## REFERENCES


1. Hageman, Jacob J., Mark S. Smith, and Susan J. Stachowiak, "Integration of Online Parameter Identification and Neural Networks for In-Flight Adaptive Control," AIAA-2003-5700, August 2003.

2. Moes, Timothy R. and Kenneth W. Iliff, *Stability and Control Estimation Flight Test Results for the SR-71 Aircraft With Externally Mounted Experiments*, NASA TP-2002-210718, June 2002.

3. Moes, Timothy R., Gregory K. Noffz, and Kenneth W. Iliff, *Results From F-18B Stability and Control Parameter Estimation Flight Tests at High Dynamic Pressures*, NASA TP-2000-209033, November 2000.

4. Davidson, Ron and Gerald Peterson, *Intelligent Flight Control: Advanced Concept Program, Final Report*, Boeing-STL 99P0040, May 15, 1999.

5. Schkolnik, Gerard S., John S. Orme, and Mark A. Hreha, *Flight Test Validation of a Frequency-Based System Identification Method on an F-15 Aircraft*, NASA TM-4704, July 1995.

6. Maine, Richard E. and Kenneth W. Iliff, *Application of Parameter Estimation to Aircraft Stability and Control: The Output-Error Approach*, NASA RP-1168, June 1986.

7. Morelli, Eugene A., "Real-Time Parameter Estimation in the Frequency Domain," AIAA 99-4043, Atmospheric Flight Mechanics Conference, Portland, OR, August 1999.

8. Klein, V., "Aircraft Parameter Estimation in Frequency Domain," AIAA 78-1344, Atmospheric Flight Mechanics Conference, Palo Alto, CA, August 1978.

9. Murray, James E. and Richard E. Maine, *pEst Version 2.1 User's Manual*, NASA TM-88280, September 1987.

10. Morelli, Eugene A., "System Identification Programs for Aircraft (SIDPAC)," AIAA 2002-4704, Atmospheric Flight Mechanics Conference and Exhibit, Monterey, CA, August 2002.

11. Smith, Mark S., Timothy R. Moes, and Eugene A. Morelli, *Real-Time Stability and Control Derivative Extraction from F-15 Flight Data*, AIAA 2003-5701, August 2003.

12. Morelli, Eugene A. and Vladislav Klein, "Accuracy of Aerodynamic Model Parameters Estimated from Flight Test Data," *Journal of Guidance, Control, and Dynamics*, Vol. 20, No. 1, January–February 1997, pp. 74–80.

13. McDonnell Aircraft Company, S/MTD Project, *STOL/Maneuver Technology Demonstrator*, Volume 1, Executive Summary, WL-TR-91-3080.

14. Crawford, Mark R., Steven Roell, Brian Hobbs, and Gerard S. Schkolnik, *STOL/Maneuver Technology Demonstrator Flying Qualities and Integrated Flight/Propulsion Control System Evaluation*, AFFTC-TR-91-29.

15. Maine, Richard E. and James E. Murray, *Application of Parameter Estimation to Highly Unstable Aircraft*, NASA TM-88266, August 1986.

16. Morelli, Eugene A., "Multiple Input Design for Real-Time Parameter Estimation in the Frequency Domain," Paper REG-360, 13th IFAC Symposium on System Identification, Rotterdam, The Netherlands, August 27–29, 2003.

# REPORT DOCUMENTATION PAGE

Form Approved
OMB No. 0704-0188



| 1. AGENCY USE ONLY (Leave blank) | 2. REPORT DATE | 3. REPORT TYPE AND DATES COVERED |
|---|---|---|
| | October 2003 | Technical Memorandum |

**4. TITLE AND SUBTITLE**

Flight Investigation of Prescribed Simultaneous Independent Surface Excitations for Real-Time Parameter Identification

**5. FUNDING NUMBERS**

745-20-00-SE-40-00-IFS

**6. AUTHOR(S)**

Timothy R. Moes, Mark S. Smith, and Eugene A. Morelli

**7. PERFORMING ORGANIZATION NAME(S) AND ADDRESS(ES)**

NASA Dryden Flight Research Center
P.O. Box 273
Edwards, California 93523-0273

**8. PERFORMING ORGANIZATION REPORT NUMBER**

H-2544

**9. SPONSORING/MONITORING AGENCY NAME(S) AND ADDRESS(ES)**

National Aeronautics and Space Administration
Washington, DC 20546-0001

**10. SPONSORING/MONITORING AGENCY REPORT NUMBER**

NASA/TM-2003-212029

**11. SUPPLEMENTARY NOTES**

Also presented at the AIAA Atmospheric Flight Mechanics Conference and Exhibit, Austin, Texas, August 11–14, 2003.

**12a. DISTRIBUTION/AVAILABILITY STATEMENT**

Unclassified—Unlimited
Subject Category 08

This report is available at http://www.dfrc.nasa.gov/DTRS/

**12b. DISTRIBUTION CODE**

**13. ABSTRACT (Maximum 200 words)**

Near real-time stability and control derivative extraction is required to support flight demonstration of Intelligent Flight Control System (IFCS) concepts being developed by NASA, academia, and industry. Traditionally, flight maneuvers would be designed and flown to obtain stability and control derivative estimates using a postflight analysis technique. The goal of the IFCS concept is to be able to modify the control laws in real time for an aircraft that has been damaged in flight. In some IFCS implementations, real-time parameter identification (PID) of the stability and control derivatives of the damaged aircraft is necessary for successfully reconfiguring the control system. This report investigates the usefulness of Prescribed Simultaneous Independent Surface Excitations (PreSISE) to provide data for rapidly obtaining estimates of the stability and control derivatives. Flight test data were analyzed using both equation-error and output-error PID techniques. The equation-error PID technique is known as Fourier Transform Regression (FTR) and is a frequency-domain real-time implementation. Selected results were compared with a time-domain output-error technique. The real-time equation-error technique combined with the PreSISE maneuvers provided excellent derivative estimation in the longitudinal axis. However, the PreSISE maneuvers as presently defined were not adequate for accurate estimation of the lateral-directional derivatives.

**14. SUBJECT TERMS**

Equation error, Intelligent flight control, Output error, Parameter identification, Stability and control derivatives

**15. NUMBER OF PAGES**

37

**16. PRICE CODE**

| 17. SECURITY CLASSIFICATION OF REPORT | 18. SECURITY CLASSIFICATION OF THIS PAGE | 19. SECURITY CLASSIFICATION OF ABSTRACT | 20. LIMITATION OF ABSTRACT |
|---|---|---|---|
| Unclassified | Unclassified | Unclassified | Unlimited |